Journal of Structural Geology 32 (2010) 755–765

Contents lists available at ScienceDirect

Journal of Structural Geology

journal homepage: www.elsevier.com/locate/jsg

Kinematics of constant arc length folding for different fold shapes

Mohammad R. Ghassemi [a,*], Stefan M. Schmalholz [b,1], Ali R. Ghassemi [c]

[a] Research Institute for Earth Sciences, Geological Survey of Iran, Azadi Sq., Meraj Ave., P.O. Box 13185-1494, Tehran, Iran
[b] Geological Institute, ETH Zurich, 8092 Zurich, Switzerland
[c] School of Electrical and Computer Engineering, Faculty of Engineering, University of Tehran, Kargar Shomali St., Tehran, Iran

ARTICLE INFO

Article history:
Received 3 October 2009
Received in revised form
17 April 2010
Accepted 8 May 2010
Available online 20 May 2010

Keywords:
Fold
Aspect ratio
Geometry
Kinematics
Constant arc length
Wrap folding

ABSTRACT

Basic mathematical functions are applied for the two-dimensional geometrical and kinematical analysis of different fold shapes. Relationships between different fold parameters are established and related to the bulk shortening taking place during folding under upper crustal conditions. The bulk shortening taking place during constant arc length folding is mathematically related to the bulk shortening during homogenous pure shear using a particular aspect ratio, which is for folding the ratio of amplitude to half wavelength and for pure shear the ratio of vertical to horizontal length of the deformed, initially square body. The evolution of the fold aspect ratio with bulk shortening is similar for a wide range of fold shapes and indicates that the fold aspect ratio allows a good estimate of the bulk shortening. The change of the geometry of individual layers across a multilayer sequence in disharmonic folding indicates a specific kinematics of multilayer folding, referred to here as "wrap folding", which does not require significant flexural slip nor flexural flow. The kinematic analysis indicates that there is a critical value for constant arc length folding between shortening values of 30–40% (depending on the fold geometry). For shortening values smaller than the critical value limb rotation and fold amplitude growth are dominating. For shortening larger than this value, faulting, boudinage and foliation development are likely the dominating deformation process during continued shortening. The kinematical analysis of constant arc length folding can be used for estimating the bulk shortening taking place during multilayer folding which is an important component of the deformation of crustal rocks during the early history of shortening. The bulk shortening is estimated for a natural, multilayer detachment fold and the shortening estimates based on the kinematic analysis are compared and supported by numerical finite element simulations of multilayer detachment folding in power-law materials.

1. Introduction

Folding, faulting and layer-parallel homogeneous shortening are three mechanisms for the deformation (shortening) of layered rocks in fold-and-thrust belts (Dixon and Liu, 1992). The research on folds and folding covers a wide range of studies focusing on different topics such as: (1) using and synthesizing mathematical functions to describe fold geometries (Currie et al., 1962; Stabler, 1968; Hudleston, 1973a; De Paor, 1996; Bastida et al., 1999, 2005; Jeng et al., 2002; Aller et al., 2004), (2) analytical solutions employing different rheologies for analyzing folding processes (Chapple, 1968; Johnson and Ellen, 1974; Johnson and Honea, 1975a,b; Biot, 1961, 1964, 1965a,b; Schmalholz et al., 2002), (3) numerical and analogue modeling of single- and multilayer folding investigating dominant wavelengths and amplification rates (Sherwin and Chapple, 1968; Hudleston, 1973a,b; Abbassi and Mancktelow, 1990, 1992; Vacas Peña and Martínez Catalan, 2004; Jeng and Huang, 2008), (4) analyzing the geometry of folded layers using the layer thickness perpendicular to layering and parallel to the fold axial plane as variables (Ramsay, 1967; Hudleston, 1973c; Ramsay and Huber, 1997), (5) investigating the kinematic implications of folding by studying the type and distribution of strain within the folded layers (Johnson and Honea, 1975a, Hudleston et al., 1996; Bastida et al., 2003, 2005, 2007; Bobillo-Ares et al., 2006), and (6) studying folds in relation to other structures such as faults, boudins, foliations and lineations (Sengupta, 1983; Mawer and Williams, 1991; Kobberger and Zulauf, 1995; Kraus and Williams, 1998; Mitra, 2003; Savage and Cook, 2003).

In this study, we apply kinematic models of constant arc length folding for estimating the bulk shortening taking place during

* Corresponding author. Fax: +98 21 66070505.;
E-mail addresses: m.r.ghassemi@gsi-iran.org, ghassemi.m.r@gmail.com (M.R. Ghassemi).
[1] Present address: Institute of Geology and Palaeontology, University of Lausanne, 1015 Lausanne, Switzerland.

0191-8141/$ – see front matter © 2010 Elsevier Ltd. All rights reserved.
doi:10.1016/j.jsg.2010.05.002

folding. The kinematic models are based on geometrical models describing observed fold shapes in profile view. Fold profiles are sections (orthogonal to the fold axis) of folded lines and their geometry can be approximated with mathematical functions. Different functions have been suggested for this purpose, which can be grouped in two major categories: non-periodic functions (Hudleston, 1973a; De Paor, 1996; Bastida et al., 1999, 2005; Aller et al., 2004; Bastida et al., 2005) and periodic functions (Currie et al., 1962; Stabler, 1968; Hudleston, 1973a; Bastida et al., 1999; Jeng et al., 2002).

This study briefly summarizes and builds on previous work on the geometry of a single folded layer in a two-dimensional profile (e.g. Stabler, 1968; Hudleston, 1973a,b; Bastida et al., 1999). The study applies basic mathematical procedures for shortening analysis of folds, and the quantities limb dip, interlimb angle, arc length, curvature, aspect ratio (i.e. ratio of fold amplitude to half wavelength) and area under the folded layer are analyzed for different fold types. The presented kinematical analysis is applied to estimate the bulk shortening that took place during folding of a natural multilayer detachment fold. The results of the kinematical analysis are compared with an analytical solution for the mechanical process of viscous single-layer folding and with numerical finite element simulations of ductile, multilayer detachment folding. The comparisons show that the kinematical folding analysis can provide good approximations for the bulk shortening during folding. Potential applications of the presented analyses for estimating the shortening, the variations of the geometry in a folded sequence, and the fold growth are discussed.

2. Fold geometry

2.1. Representing fold geometries with mathematical functions

Fitting all fold shapes with one type of mathematical function is not suitable because geometries of natural folds vary significantly. For example, methods for fitting folds with ellipses (Mertie, 1959) are unsuitable for an accurate representation of fold shapes and many common fold styles (e.g. chevron folds) cannot be represented at all.

Representing fold shapes with Fourier series received most attention (see Norris, 1963; Chapple, 1964, 1968; Harbaugh and Preston, 1965, Stabler, 1968; Hudleston, 1973a; Ramsay and Huber, 1997) because many folds are naturally periodic. The Fourier analysis of fold shapes is useful for sinusoidal fold shapes (see Stabler, 1968; Hudleston, 1973a), however, it has some drawbacks when applied to other fold shapes (see Bastida et al., 2005).

Several studies (Bastida et al., 1999; Aller et al., 2004; Bastida et al., 2005; Lisle et al., 2006) suggested a range of functions for representing fold shapes. Bastida et al. (1999) suggested a power function:

$$\frac{y}{y_0} = \left(\frac{x}{x_0}\right)^n \tag{1}$$

in which n characterizes the fold shape, x_0 and y_0 are the coordinates of the inflexion point on the fold limb, and y and x are the vertical (i.e. parallel to the fold axial plane) and horizontal coordinates, respectively. In order to have a common coordinate system[2] and to analyze the fold limb between an inflection point at the origin of the coordinate system and the fold hinge we use a similar function:

$$y = 4\frac{A}{w}(1-(1-x)^n), \tag{2}$$

where A and w are the amplitude and wavelength of the fold, respectively. This equation does not have the inconveniences of Eq. (1) which are described in Bastida et al. (2005). Equation (2) can be modified to a function for the variable p which is the aspect ratio of the fold and defined as the ratio of fold amplitude to half the fold wavelength (Twiss, 1988):

$$y = 2p(1-(1-x)^n). \tag{3}$$

For $n = 1$ Eq. (3) is

$$y = 2px, \tag{4}$$

and represents ideal chevron folds.

For $n = 2$ Eq. (3) is

$$y = 2p\left(2x - x^2\right), \tag{5}$$

and represents parabolic folds.

Applying a power of 0.5 to the right term in braces in Eq. (5) results in

$$y = 2p\left(2x - x^2\right)^{0.5}, \tag{6}$$

and represents ellipsoidal folds.

Using $n > 2$ in Eq. (3) produces double hinge fold shapes (see Table 1).

Equations (3)–(6) and the Fourier series for the first harmonic can be used to describe a wide variety of fold shapes. These equations are not based on one type of function and, therefore, lack the continuity of fold shapes which is for example a feature of the power function of Eq. (1) (Bastida et al., 1999). However, because of the wide diversity of natural fold shapes we represent here basic fold shapes with specific functions that best fit the observed fold shape (see Table 1).

Cuspate folds are not represented with any specific function because all functions listed in Table 1, except the linear function, represent different shapes of cuspate folds when they are mirrored against the chord of the fold's quarter wavelength.

2.2. Basic geometrical implications of fold shapes

The interlimb angle, i, of upright symmetrical chevron folds is related to their aspect ratio, p:

$$i = 2\arctan\frac{1}{2p}. \tag{7}$$

Ghent and Hansen (1999) used an equation similar to Eq. (7), however, what they termed fold wavelength is in fact the fold's half wavelength. The interlimb angle is increasingly smaller for sinusoidal, parabolic and double hinge folds for the same value of p. The maximum dip of the fold limb, l, at the inflection point of upright

Table 1
General functions for different fold geometries used in this study for analyzing fold geometry and kinematics.

Fold type	General function
Chevron	$y = 2px$
Sinusoidal	$y = 2p\sin(\pi/2x)$
Parabolic	$y = 2p(2x - x^2)$
Ellipsoidal	$y = 2p(2x - x^2)^{0.5}$
Double hinge (box)	$y = 2p(1-(1-x)^n)$; $n > 2$

[2] Following Hudleston (1973a) and Ramsay and Huber (1997), this paper assumes the y axis of the coordinate system passing through inflection point of the fold and parallel to the axial surface of the fold. The x axis also passes through the inflection point, and is perpendicular to the y axis.

symmetrical folds can be calculated from the interlimb angle ($l = 90 - i/2$). Equation (7) is used for calculating the value of p as function of the interlimb angle and the limb dip for symmetric chevron folds. For the other fold types, equations similar to Eq. (7) can be used (Fig. 1).

In mechanical models for folding of linear viscous single layers, the evolution of the fold's aspect ratio, p, with increasing horizontal bulk shortening is different for different viscosity ratios between the layer and the embedding matrix (Fig. 2-A; Schmalholz and Podladchikov, 2000; Schmalholz, 2006). The reason is that the smaller the viscosity ratio is the larger is the component of arc length shortening and layer thickening. For large viscosity ratios (>about 500) single-layer folding is close to constant arc length folding because layer thickening is very small. However, the evolution of p with increasing interlimb angle is identical for all viscosity ratios because the fold shape is assumed to be sinusoidal in the analytical solution of Schmalholz (2006) (Fig. 2-B). This analytical solution was compared with two-dimensional numerical simulations of viscous single-layer folding and the analytical amplification prediction agreed well with the numerical results (Schmalholz, 2006). Therefore, the kinematical curve of p versus the interlimb angle for sinusoidal fold shapes (Fig. 1) is a good approximation for the amplification of natural single-layer folds.

2.3. Curvature and dip distribution along fold profile

The pattern of curvature variation along the folded line and the sign of curvature can be used to define all fold types. The fold hinge is the point of maximum curvature and the inflection point is the point of minimum (zero) curvature, and also the point where the curvature changes sign. The curvature can be used for estimating the strain ratio in different areas of the fold during buckling (see Ramsay, 1967, p. 391; Bobillo-Ares et al., 2006) and for calculating tangential longitudinal strain (Bobillo-Ares et al., 2000). The first derivative of the function defining the fold shape is the limb dip and can be used for estimating the angular shear strain in flexural slip folding (see Ramsay, 1967, p. 393).

Ramsay (1967, p. 347) describes the curvature variation across a folded line as a quantity that can be used to define different types of fold shapes (see also Chapple, 1969). Bastida et al. (2005) also considered the curvature, κ, as a basic parameter in the kinematical analysis of folding:

$$\kappa = \frac{1}{\rho} = \frac{f''(x)}{\left[1 + f'(x)^2\right]^{1.5}} \tag{8}$$

where ρ is the radius of curvature, and $f'(x)$ and $f''(x)$ are the first and second derivatives of $f(x)$, respectively. In order to analyze the dip pattern and curvature distribution we plotted (Fig. 3) the profile of the folded line together with the first derivative and the curvature (Eq. (8)) of the function describing the fold shape.

Chevron folds are different from other folds in having a long inflection zone relative to their hinge zone. The curvature is minimal (zero in ideal chevron folds) in most of the limb making the definition of an inflection point difficult. Equation (4) describing chevron folds provides the limb dip $l = \arctan(2p)$ and the interlimb angle $i = 180 - 2\arctan(2p)$. For all other fold types a similar relation, namely $i = 180 - 2l$, is applicable. Sinusoidal folds have both the highest gradient in curvature in the limb and the highest curvature in the hinge zone compared to parabolic and ellipsoidal folds of the same aspect ratio (Fig. 3). The maximum dip at the inflection point is $\arctan(p\pi)$.

A problem of using non-periodic functions to define fold shapes is the discontinuity in curvature at the inflexion points. Since the curvature of parabolic, ellipsoidal and double hinge folds does not go to zero (see Fig. 3) a combination of these functions cannot produce ideal fold shapes at the inflection point where zero curvature is required in joining the quarter wavelength sections of several anticline–syncline pairs. For these cases the point of curvature sign change can be considered as the inflection point. Parabolic folds have less curvature at the hinge zone as compared to sinusoidal folds, but have a higher curvature relative to ellipsoidal folds of the same aspect ratio (see Fig. 3). The maximum curvature of parabolic folds is twice the maximum curvature of ellipsoidal folds of the same aspect ratio. The maximum dip at the inflection point of parabolic folds equals $\arctan(4p)$.

For $p = 0.5$ the shape of an ellipsoidal fold is a semicircle and the curvature is constant in the limb (Fig. 3). However, with increasing values of p the curvature becomes more differentiated in the hinge zone. The maximum dip at the inflection point for all ideal

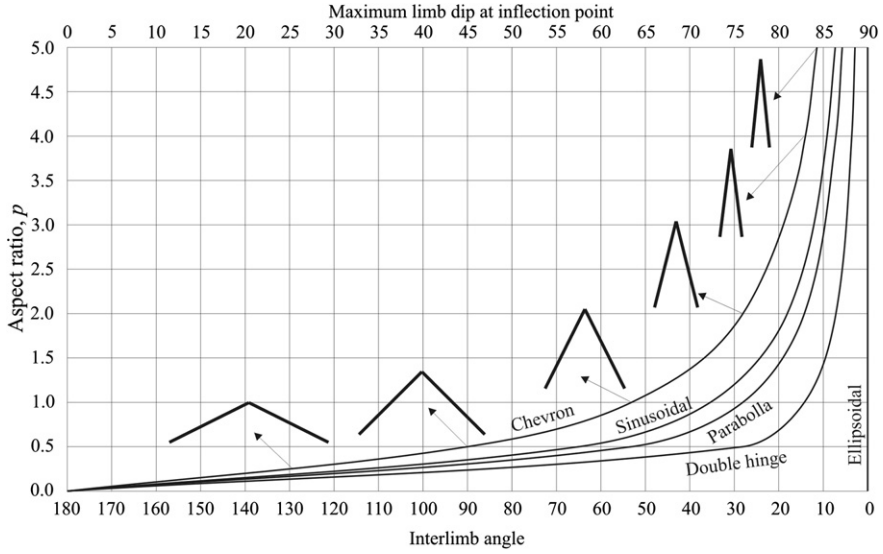

Fig. 1. Diagram of interlimb angle and maximum limb dip of different fold shapes versus the aspect ratio, p (i.e. ratio of fold amplitude to half the wavelength), of the folds. Note the constant interlimb angle and limb dip of ellipsoidal folds plotted at the right of the diagram.

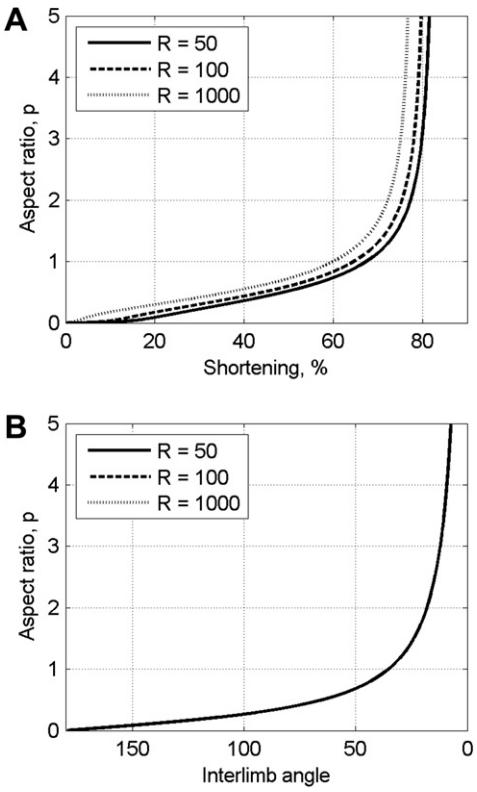

Fig. 2. Finite amplitude solution for linear viscous single-layer folding (Schmalholz, 2006). A) The fold aspect ratio, *p*, versus the horizontal shortening for different values of the viscosity ratio, R. Folding with a high viscosity ratio of 1000 is close to folding with constant arc length. Folding with smaller viscosity ratios includes a considerable component of arc length shortening which is visible in smaller aspect ratios at equal amounts of shortening. B) In the space aspect ratio, *p*, versus interlimb angle all lines for different viscosity ratios collapse because the fold shape is always sinusoidal independent on the amount of arc length shortening and corresponding layer thickening.

ellipsoidal folds equals 90°. Therefore, ellipsoidal arcs are the best curves to define isoclinal folds.

Double hinge folds have a separate point of maximum curvature in each limb and the curvature declines to zero at the midpoint between the two hinges. The magnitude of curvature at the hinges and the dip of the limb at the inflection point increases with an increasing value of the power, *n*, of the function describing the fold shape. Box folds can be considered as members of the double hinge fold family.

3. Fold kinematics

3.1. Bulk shortening during constant arc length folding

Following early works of, for example, Chamberlin (1910), Ramsay's method (1967, p. 387) allows quantifying the bulk shortening (i.e. the horizontal shortening between two fold hinges) resulting from folding. Ramsay defined the maximum shortening of a concentrically folded competent layer as

$$100(2\pi t - 4t)/2\pi t = 36\%, \tag{9}$$

where t is half the thickness of the layer, and also the radius of curvature for the semicircle defining the fold shape. The shortening value of 36% in Eq. (9) agrees with the results for shortening in this study for an ellipsoidal fold with an aspect ratio of 0.5 (Fig. 4).

The arc length, L, of a folded line can be calculated with

$$L(x) = \int_0^{w/4} \left(\sqrt{1 + (f'(x))^2}\right) \mathrm{d}x, \tag{10}$$

where w is the wavelength of the fold. Assuming a constant arc length, L, during folding, the value of L can be used for estimating the bulk shortening, e, perpendicular to the axial surface with

$$e = \frac{l_f - l_i}{l_i} = \frac{\frac{w}{4} - L}{L} \tag{11}$$

For chevron folds the shortening is related to the aspect ratio through the relation

$$p = 0.5\left(\frac{1}{(1+e)^2} - 1\right)^{0.5} \tag{12}$$

Similar relations exist between the shortening, e, and the aspect ratio, R, of a body with an unstrained ratio of 1 (i.e. square) and with the same mechanical property as the matrix that has been deformed without area change (pure shear in two dimensions under plane strain):

$$R = \frac{1}{(1+e)^2}, \quad e = \frac{1}{R^{0.5}} - 1, \tag{13}$$

from which relations can be established between p and R:

$$p = 0.5(R-1)^{0.5}, \quad R = 4p^2 + 1 \tag{14}$$

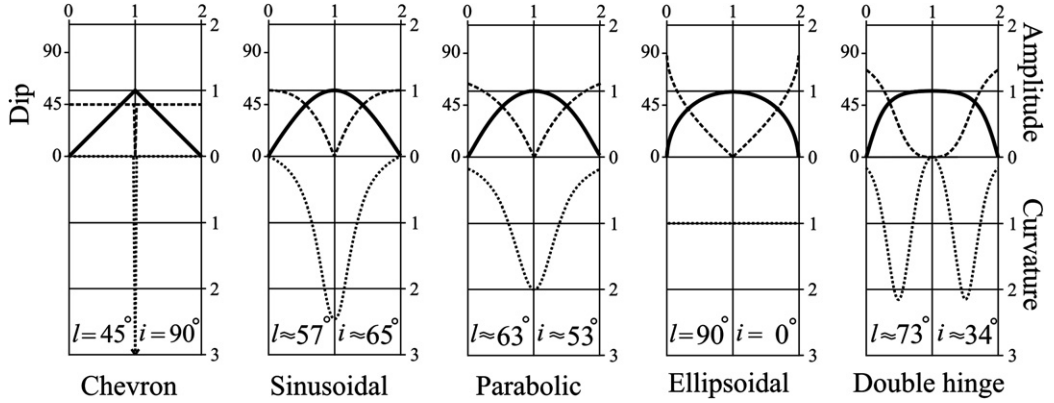

Fig. 3. Dip and curvature diagrams for different fold shapes with an aspect ratio of 0.5. The function applied for double hinge fold has a value $n = 4$. Limb dip at inflection point, *l*, and interlimb angle, *i*, are shown at the bottom of each diagram.

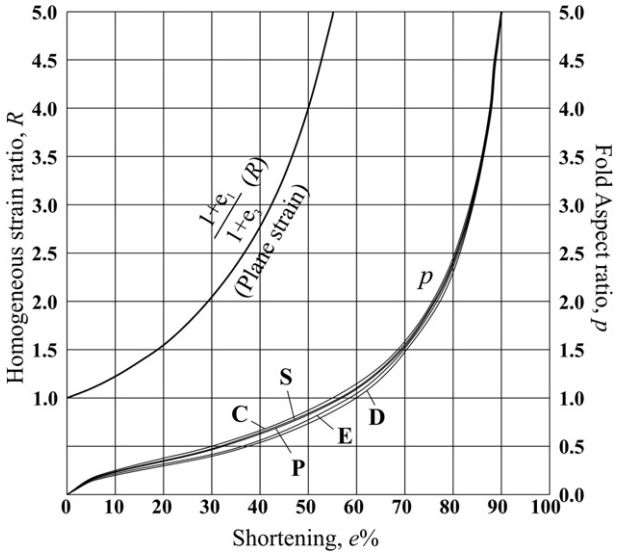

Fig. 4. Variation of fold aspect ratio, p, and homogeneous strain ratio with shortening. Note a maximum variation of shortening (about 10%) between different fold shapes at an aspect ratio of about 0.5. (C) Chevron, (S) sinusoidal, (P) parabolic, (E) ellipsoidal, (D) double hinge of function power $n = 4$.

Using the above equations and introducing different values for the aspect ratio, the shortening of folds exhibiting different fold types can be calculated (Fig. 4). Currie et al. (1962) presented a diagram similar to Fig. 4.

The diagram in Fig. 4 can serve as upper limit for fold amplification diagrams (see Ramsay, 1967, p. 379; Hudleston, 1973a,b) when a significant viscosity ratio between the folded layer and the embedding matrix minimizes layer-parallel shortening. The calculated values of shortening are close for specific aspect ratios of different fold shapes, and show a maximum variation of about 10% at $p \approx 0.5$ (see Fig. 4). Increase of the aspect ratio accelerates with increasing shortening values indicating a decrease of the folding process as the major process of shortening.

The change in limb dip with shortening has also a dynamic implication, because the increasing limb dip causes a rotation of the normal to the folded layers towards the direction of the maximum principal stress (i.e. the compression direction). This increases the ratio of normal to tangential stress which in turn prohibits layer-parallel slip and, therefore, flexural slip folding.

Distortion, translation and rotation occur both in homogeneous pure shear and folding, however, homogeneous pure shear mostly involves distortion, while folding generally requires a major component of rigid body deformation including translation and rotation. Such difference is essential during folding of multilayered rocks with varying viscosities. Stiff layers tend to deform mostly by rigid body deformation, and the particle path they develop differs from the one for homogeneous strain in their confining medium. The resultant of these paths defines the bulk deformation of the multilayered rocks.

We compare the bulk shortening resulting from a simple model of chevron folding with the bulk homogeneous shortening due to pure shear (Fig. 5). The aspect ratio of the folded multilayers is

$$R_f = \frac{T_a}{M}, \tag{15}$$

where T_a and M are the apparent thickness of the folded layers parallel to the axial plane and half the wavelength of the folds, respectively. The apparent thickness of the layers is

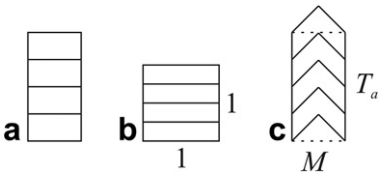

Fig. 5. Comparison of deformations resulting from homogeneous pure shear (a) and from symmetrical chevron folding (c); (b) represents the initial geometry before shortening. The area left over from up-folding of layers at the bottom is balanced with the area projected at the top. Shortening in both cases is 30%, and of plane strain character (constant area or constant layer thickness).

$$T_a = \frac{1}{\cos l}. \tag{16}$$

From Eq. (7) and the relation between the interlimb angle, i, and limb dip, l, we can use the following equations to calculate the apparent thickness:

$$l = 90 - \frac{i}{2}, \quad T_a = \frac{1}{\sin\frac{i}{2}} = \frac{1}{\sin\arctan\frac{1}{2p}}. \tag{17}$$

Using Eq. (12) and $\lambda' = 1/(1+e)^2$ we get

$$T_a = \frac{1}{\sin\arctan\frac{1}{(\lambda'-1)^{0.5}}} \tag{18}$$

which can be modified into

$$T_a = \frac{\left(1+\frac{1}{\lambda'-1}\right)^{0.5}}{(\lambda'-1)^{-0.5}} = \left(1+\frac{1}{\lambda'-1}\right)^{0.5}(\lambda'-1)^{0.5} = (\lambda')^{0.5}. \tag{19}$$

For an initial aspect ratio of 1 we get

$$M = 1 + e = \left(\frac{1}{\lambda'}\right)^{0.5}, \tag{20}$$

and, therefore, the aspect ratio of folded multilayers is

$$R_f = \frac{T_a}{M} = \frac{(\lambda')^{0.5}}{\left(\frac{1}{\lambda'}\right)^{0.5}} = \lambda' = \frac{1}{(1+e)^2}. \tag{21}$$

Equation (21) may also simply be inferred from the condition of no area change, and constant arc length folding. Comparing Equations (21) and (13) for the aspect ratio of homogeneous shortening shows that the bulk shortening taking place during folding in our model is equal to the homogeneous shortening for pure shear. However, the infinitesimal strains in different areas of the folded layers are different, and the particle path and velocity field also deviates from that of homogeneous strain. For a detailed mechanical analysis of the velocity field for a chevron fold model see Pollard and Fletcher (2005; pp. 177–182).

The strain within the layers of a chevron fold can be analyzed with two end members: (i) the strain in the whole layer (Ramsay, 1967, 1974), and (ii) the strain in the hinge zone (Bastida et al., 2007). As shown in Fig. 5, a bulk simple shear of value $\gamma = \tan l$ symmetrically affects both limbs of the chevron folds. This strain can occur either by shear parallel to the axial plane or by shear parallel to the layering and a rotation equal to the angular shear. The first case is almost impossible because the shear plane is perpendicular to the maximum shortening direction. Shear parallel to the layering can occur either by slip along the layer contacts

(flexural slip) or bulk shear within the layer (flexural flow). The sum of these two shear strains should equal the bulk layer-parallel simple shear of each limb. Where slip along the layer interfaces is easy because of low friction and/or low cohesion between the layers, or the presence of incompetent layers between competent layers, the flexural flow has a lower share of the bulk shear. Where interlayer slip is difficult, flexural flow dominates over flexural slip. Following the suggestion of Hudleston et al. (1996) that flexural flow is scarce in natural folds, the flexural slip should occur when the folded sequence is composed of alternating high and low viscosity layers, or most of the shear should take place in the hinge area of chevron folds.

3.2. Kinematic implications

Field study of folds usually involves measurements of bedding and/or foliation attitudes. These data are used to describe spatial characteristics of the folds, such as interlimb angles. Having access to data from geological maps, aerial photographs and satellite images enables measuring the wavelength of folds. However, without subsurface data it is difficult to evaluate fold amplitudes and, therefore, the aspect ratio of folds. Assuming that the natural fold geometry can be represented by one of the fold shapes considered in this study, and having data for the interlimb angle or the maximum limb dip, we can use diagrams similar to that shown in Fig. 1 to estimate the fold's aspect ratio. From the aspect ratio we can estimate the amplitude of a single fold or a fold train or the shortening that took place during folding. The method can be used in areas of detachment folding such as the Zagros simply folded belt of Iran to analyze fold geometries and kinematics. This method can also be used to estimate shortening due to folding on terrestrial planets such as Venus, where erosion and deposition are not active, and fold geometries might be deduced from surface topography (Connors, 1995). This is especially practical where it is possible to produce a slope map of the planet surface using remotely developed topographic maps.

Another implication of the analysis is that when the bulk finite strain is homogeneous in the direction of shortening, we would expect that the shortening in both limbs of asymmetric folds is equal. This helps to evaluate shortening in the long limb of asymmetric folds and extrapolate it into the short limb of the fold, and *vice versa*.

It is instructive to compare the fold shape, the length of the folded layer, and the area under the fold profile in a simple diagram (Fig. 6). Cuspate folding produces the smallest area in the core of the fold, while chevron, sinusoidal, parabolic, ellipsoidal and double hinge folding produce larger areas in their cores. A similar sequence of fold types may appear in a folded section of multilayers from the core of the fold in an outward direction. Disharmonic folds that developed due to space problems in parallel folding above detachments show chevron folds and even isoclinal folds in their core (Mitra, 2003).

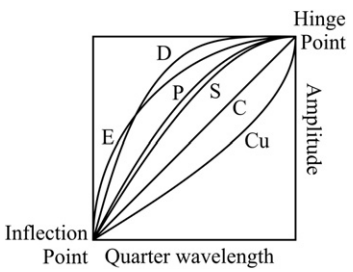

Fig. 6. Comparison of fold shape and area under the fold for different fold shapes with aspect ratio of 0.5. (Cu) cuspate, (C) chevron, (S) sinusoidal, (P) parabolic, (E) ellipsoidal, (D) double hinge (for $n = 4$).

When shortening is more or less constant in direction parallel and perpendicular to the axial plane, the fold geometry across the layered section and across the fold train should vary and compensate this shortening continuity. In the case of parallel folding, the available space decreases towards the fold's core. This leads to a decrease in wavelength but does not affect the amplitude (Fig. 7). Ramsay's classification (p. 365, 1967) also requires a decrease of the inner arc curvature for the class 1 of folds (including parallel folds). The situation is opposite in anticline–syncline pairs and, therefore, the differential shortenings may cancel out along a fold train. In a single fold (e.g. anticline), however, the change in wavelength alters the aspect ratio of the fold and, therefore, affects shortening. In this case, when shortening has to be constant, it is distributed with an increase in wavelength as well as a change of fold geometry. This results generally in disharmonic folding.

Disharmonic folding as described here also prevents flexural slip that is required for constant limb lengths across the folded sequence. In this mode of folding the outer layers of the folded sequence are increasingly longer and in fact wrap around inner layers. This may be named "wrap folding", which contrasts with folding accommodated by simple shear between and within the layers.

It is also instructive to compare the profiles of different fold shapes for their potential in conserving the layer thickness at the inflection point and the hinge zone (Fig. 8). This comparison indicates that for parallel folding (i.e. folding with constant thickness), chevron folds best conserve the fold geometry in terms of amplitude, wavelength and fold shape with a minimum matrix area in hinge zone. Chevron folds also do not decrease the limb thickness for similar folding (i.e. folding with constant fold shape). Sinusoidal and parabolic folds produce more extra matrix area in their hinge zone for parallel folding when the fold type is constant; for similar folding they require some thinning of the limbs at the inflection points. Ellipsoidal and double hinge folds produce very large extra space in their hinge zones for parallel folding and they require a large amount of thinning in their limbs for similar folding. Cuspate folds produce extra space both in their limbs and in their hinge zones for parallel folding. However, for similar folding the limb thickness is constant except for some thinning in the hinge zone.

A decrease of wavelength requires that the amplitude also decreases in order to keep the aspect ratio constant. Otherwise the fold type changes into a type that accommodates less shortening and needs less space. This is in agreement with conclusions of previous studies (Carey, 1962; Goguel, 1962; de Sitter, 1964; Dahlstrom, 1990; Johnson and Honea, 1975b; Mitra, 2003) indicating that the core of concentric folds is a favored site for the development of chevron folds.

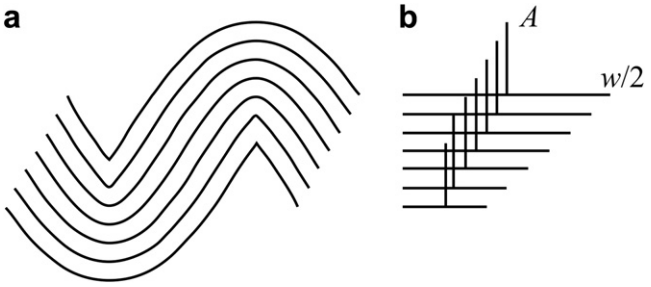

Fig. 7. (a) Change in fold profile geometry in a layered sequence. (b) Amplitude and half wavelength of the layers. The amplitude of the folds is constant and the half wavelength decreases linearly towards the fold's core in the anticline, which is compensated by an increase in the half wavelength outward in the neighboring syncline. Note the almost linear decrease of limb length towards the core.

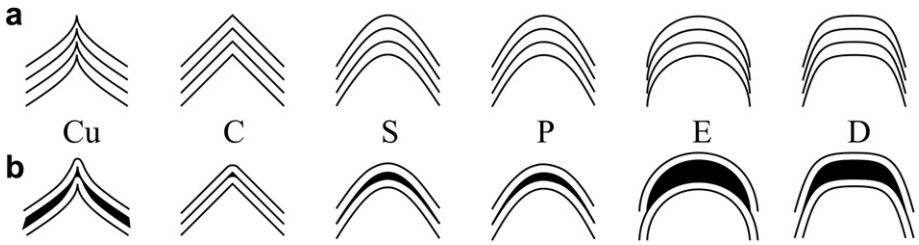

Fig. 8. Conservation degree of folded layer thickness parallel to axial plane (a), and perpendicular to layering (b). Note the extra space (black area) that is present between folded layers in parallel folding. (Cu) cuspate, (C) chevron, (S) sinusoidal, (P) parabolic, (E) ellipsoidal, (D) double hinge (with $n = 4$).

If folding starts at depth and propagates up section it is possible that folding starts as chevron folding at depth and varies into broader types of folds up section. It is also possible that, as deduced from the usually acute angle of chevron folds by Bastida et al. (2007), these core folds may evolve form more rounded fold shapes.

4. Application to natural and synthetic multilayer folds

We applied the kinematic models to a natural multilayer detachment fold. A series of mesoscopic folds in dolomitic limestone layers of the Elika Formation (Triassic) outcropped in the north central part of the Alborz range (Figs. 9 and 10) provides an example for the change of the geometry of folded layers through the folded sequence. The folded sequence exhibits a minor fault in the core. The fold geometry changes from chevron through sinusoidal to double hinge fold shapes from bottom to top of the folded sequence. The bulk shortening was calculated between two reference lines perpendicular to the original layering (Fig. 9). The reference lines were selected closest to the main anticline in the section to minimize the amount of variation in the shortening calculation. The calculated values of shortening increase slightly up section, however, the variation in shortening values is small (Fig. 10). The half wavelength of the folded layers, however, increases considerably (about 5 times) up the section (Fig. 9). Shortening is almost constant across the section indicating that multilayer folding accommodates space and shortening with both a change in fold shape from chevron to double hinge and a decrease in aspect ratio (because of an increase in the distribution of deformation and an increase of wavelength).

The natural detachment fold in Fig. 9 is localized and only a single multilayer fold was observed in the field (no additional folds are present along the layering). Numerical simulations of multilayer detachment folding were applied to generate a multilayer fold similar to the one observed. The applied numerical algorithm is based on the finite element method, can model linear viscous and power-law rheologies, and is described in detail in Schmalholz et al. (2008). For all simulations, all layers were initially flat, but had a small geometrical step of 1/25th of the layer thickness in the middle of the model domain to trigger folding. For the linear viscous material the viscosity ratio between layers and matrix was 100. For the power-law material the viscosity ratio was 100 and layers and matrix had a power-law exponent of 5. Initially, the distance between individual layers was 1/10th of the layer thickness. The numerical simulations of multilayer detachment folding with linear viscous rheology show that there is always lateral fold propagation during shortening, although the initial geometrical perturbation is localized (Fig. 11). Therefore, it is not possible to generate a single, localized multilayer fold as the one shown in Fig. 9. If a non-linear, power-law rheology is used, then folding is localized and a single fold can develop (Fig. 12). This indicates that the rheology during the formation of the observed, localized multilayer fold is better described with a power-law rheology than with a linear viscous rheology. The power-law rheology yields larger amplification rates than the linear viscous rheology for the same effective viscosity ratio and, therefore, folding is closer to constant arc length folding.

Estimating the horizontal shortening from the numerical multilayer fold (from Fig. 12) assuming constant arc length

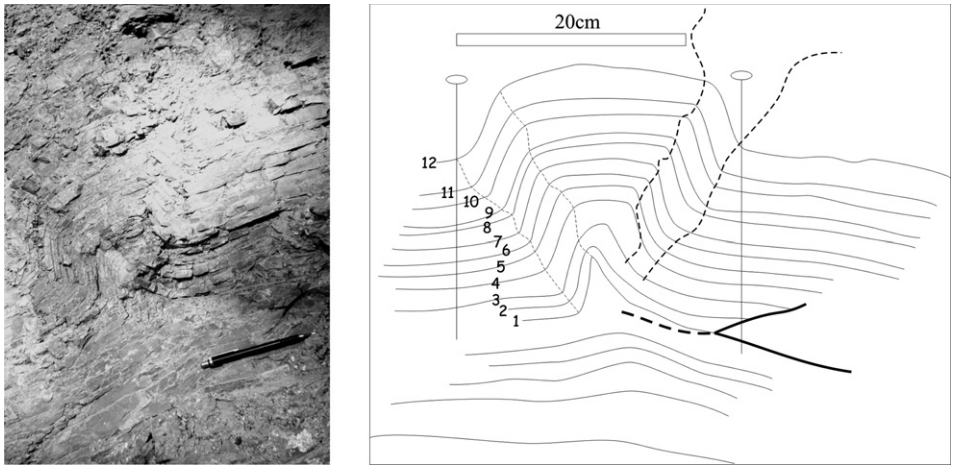

Fig. 9. Left picture shows a folded sequence of dolomitic limestone (Elika Fm.) in the north central Alborz range, Iran. Right panel shows a sketch of the fold geometry. Bold lines indicate a fault. Dashed lines in the left part indicate the axial trace of the folded layers. Dashed lines in the right part indicate a zone of slight cataclasis in the folded layers. Vertical straight lines bound parts of the folded layers that are used for calculating the shortening assuming a constant arc length during folding. The sketch illustrates also the change in fold type across the multilayer fold.

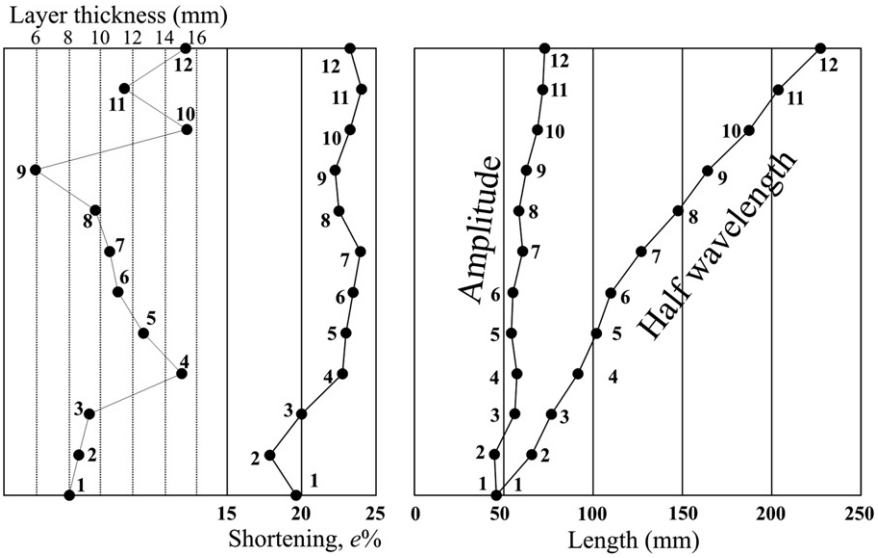

Fig. 10. Variation of the estimated shortening, the amplitude, half the wavelength and the layer thickness across the folded sequence in Fig. 9. Numbers in the panels indicate the layer of the folded sequence in Fig. 9. Note the almost constant shortening and amplitude in contrast to the linear increase of the half wavelength across the sequence. The layer thickness appears not to have any pronounced effect on the amplitude or wavelength.

folding provides a minimum estimate, and the true horizontal shortening known from the numerical simulation is slightly larger (Fig. 13). For the particular numerical simulation shown in Fig. 13 the true shortening is about 5% larger than the estimated shortening. Also, the shortening of the individual layers is very similar although their individual fold shapes are different. This agrees with the distribution of shortening estimates for the observed fold (Fig. 10).

The numerical simulations indicate that estimates of horizontal shortening for localized multilayer folds based on the constant arc length assumption provide minimum shortening estimates. These estimates are likely not much smaller than the true shortening value for high viscosity ratios because localized multilayer folds are likely formed in power-law multilayers with a small amount of layer thickening.

We calculated the variation of the area, B, under the folded surface for symmetrical chevron folds with increasing shortening (decreasing wavelength and increasing aspect ratio) with

$$B = \frac{M}{2}\left(0.25 - \frac{M^2}{4}\right)^{0.5} \tag{22}$$

where M is half the wavelength of the fold.

The crestal uplift of the fold can be maximal $2A$ when the detachment surface allows no downward movement of the folded layers. The variation in amplitude, A, is an indicator of crestal uplift in active folds and can be calculated with

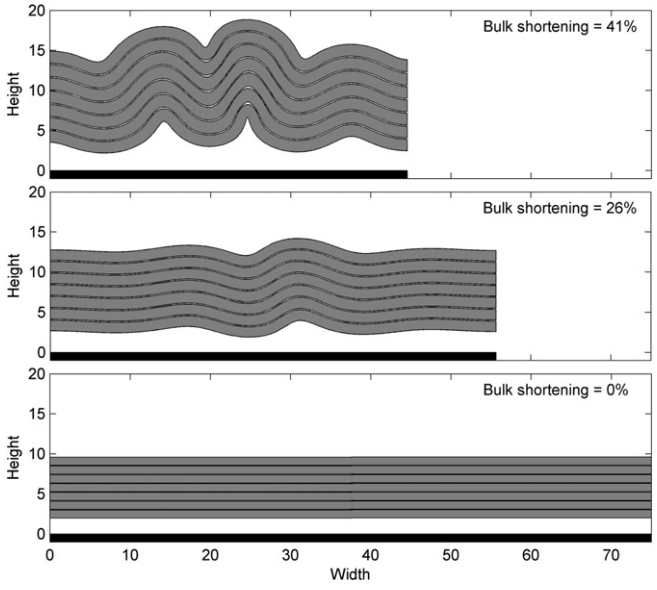

Fig. 11. Numerical simulation of multilayer folding above a detachment for a viscosity ratio of 100 and a power-law exponent of 1 (i.e. linear viscous). Gray = stiff layers, white = weak matrix and black = base with no vertical movement. Several folds develop due to lateral fold propagation.

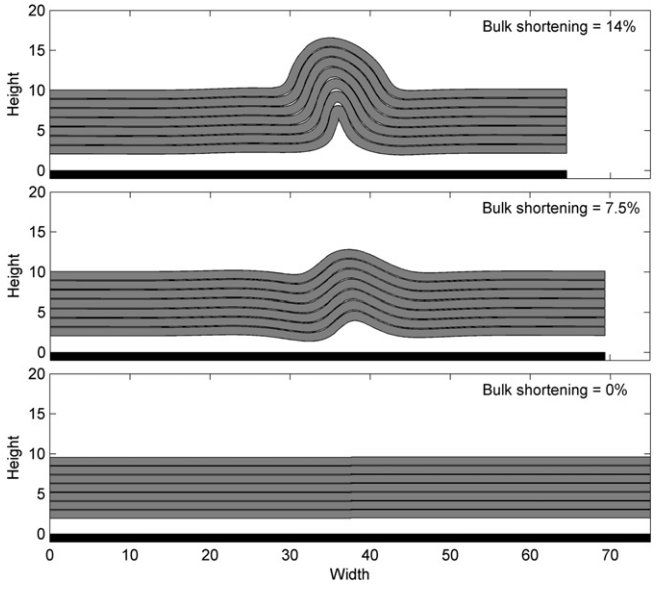

Fig. 12. Numerical simulation of multilayer folding above a detachment for a viscosity ratio of 100 and a power-law exponent of 5. Gray = stiff layers, white = weak matrix and black = base with no vertical movement. Only one single fold develops due to the localization of the deformation caused by the non-linear power-law rheology.

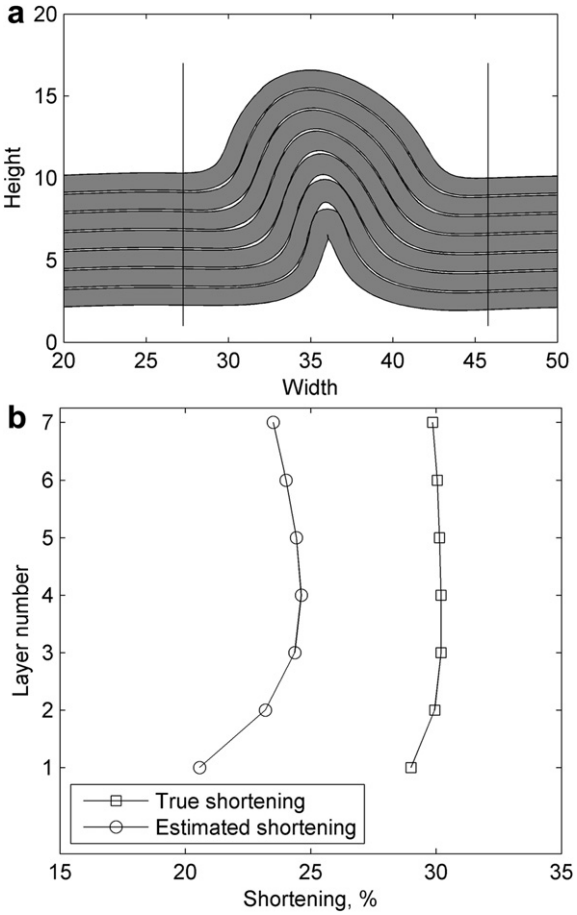

Fig. 13. A) Numerically generated fold shape. The two vertical lines indicate the reference lines for the shortening calculation. B) Estimated and true (known from numerical simulation) horizontal bulk shortening for each of the seven layers. The estimated shortening value assumes constant arc length folding and is therefore smaller than the true shortening value which includes a certain amount of arc length shortening and corresponding layer thickening.

$$A = \left(0.25 - \frac{M^2}{4}\right)^{0.5} \tag{23}$$

The analysis (Fig. 14) shows that folding produces a maximum area below the folded sequence at a shortening of about 29% (interlimb angle of about 90°). Clearly, this maximum value occurs at different amounts of shortening for fold types other than chevron. For a comparison of the area under profiles for different fold shape types see Bastida et al. (2005). The variation in area below folded layers may be a reason for the cessation of folding as the main mechanism for shortening after some amount of deformation, and may explain the onset of faulting. Chapple's (1968) results may also be another evidence for the impact of the variation of the area in fold cores with shortening. He describes that at a limb dip of about 65° an important change in the style of the deforming fold occurs: the medium (matrix) ceases to move into the crestal regions of anticlines and starts to be extruded from between the fold limbs. de Sitter (1956, 1958) predicted the cessation of chevron folding at an interlimb angle of 50–60°. He also suggested that shortening of the crust by chevron folding by more than 50–65% is unlikely. Similar conclusions may be reached theoretically for the other types of fold shapes.

The analysis of the area below the folded layer (Fig. 6) has implications for the rock volume available for erosion in an exposed

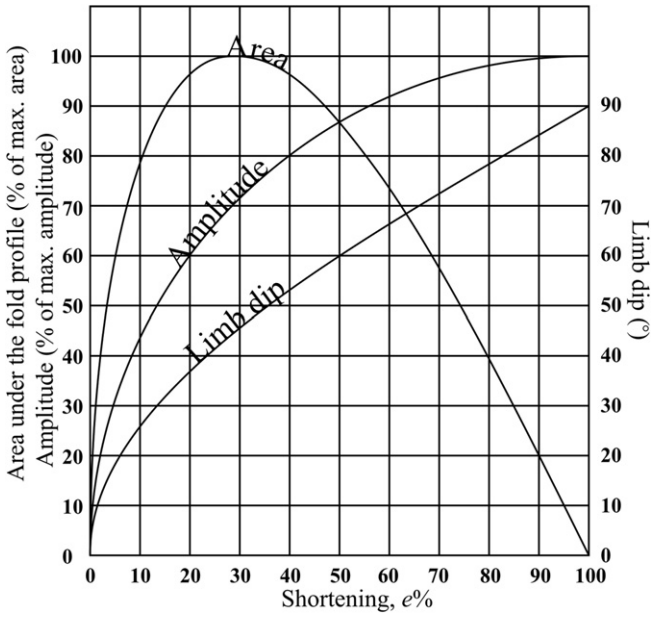

Fig. 14. Change in limb dip, amplitude (crestal uplift) and area under the fold profile of symmetric upright chevron folds with shortening.

active fold and can help to understand the rise and demise of relief in folded terranes. Increasing the relief of folded rocks to a maximum can increase the solid load in antecedent rivers across active folds while the riverbed gradient is being decreased as the upstream limb of the fold is tilted. This may define a critical point at which the river is either defeated or overcomes the fold uplift.

The limb dip of upright symmetric chevron folds can also be calculated as a function of shortening:

$$l = 90 - \arctan\left(\lambda' - 1\right)^{-0.5}. \tag{24}$$

The above relation is shown in Fig. 14 (compare with Fig. 5 in Ramsay, 1974). The relation is valid for the limit when the ratio of layer thickness to limb length approaches zero (see Fig. 7-112 in Ramsay, 1967).

Shortening as a function of limb dip is given by:

$$1 + e = \left(1 + \tan^2 l\right)^{-0.5}. \tag{25}$$

The increase of limb dip and amplitude of chevron folds with increasing shortening indicates that limb dip and amplitude initially grow fast up to a shortening value of about 30% (aspect ratio of about 0.5 and limb angle of about 45°) and for larger shortening values their growth rates decrease gradually (Fig. 14). The curve in Fig. 14 also provides the limb rotation rate, which has an impact on the geometry of growth strata above active folds, on angular unconformities between these strata and on the flight of fluvial terraces (for an analysis of this type see Scharer et al., 2006).

5. Discussion and conclusions

It is useful for the regional kinematical analysis of folded terranes to evaluate the bulk shortening that would have taken place during folding with constant arc length. The kinematical analysis allows calculating the fold arc length and, therefore, the bulk shortening for different fold shapes.

This study indicates that bulk shortening taking place during constant arc length folding is very similar for different fold

geometries. The maximum difference in shortening is about 10% at an aspect ratio of about 0.5 between shortening values of 30–40%. This small variation in shortening values indicates that the aspect ratio of folds can serve as a useful estimate of shortening due to constant arc length folding.

The simple relationships between the fold aspect ratio, interlimb angle, limb dip, shortening and other parameters presented in this study are suitable for the regional analysis of fold geometries and kinematics when remote data are combined with field studies, or when specific information about the folded terrain is available.

The geometrical and kinematical comparison of shortening, fold shape, limb dip, arc length and area below the profile for different fold types provides useful information on:

- cross sectional variation of fold geometry in different layers, especially for detachment folding of parallel type,
- rate of limb rotation, volume of material available to erosion, and crestal uplift of active folds; parameters that can be applied in studies of the geomorphological evolution of exposed folds and of the evolution of growth strata over active folds, and
- potential of different fold geometries for conserving the layer thickness perpendicular to the layering in parallel folding, and parallel to the axial plane in similar folding.

The change in fold geometry across layers in some disharmonic fold systems is an alternative mechanism of folding that may be termed "wrap folding" which accommodates space variations without requiring simple shear parallel to folded layers (flexural slip or flexural flow).

One result of this study is the definition of a critical value of shortening for folding under rheological conditions of the upper crust: constant arc length folding is dominant for shortening values smaller than about 30–40% (i.e. aspect ratio of about 0.5), but for larger shortening values faulting and foliation development may dominate during continued shortening. Clearly, a significant component of shortening may occur prior and during the folding which may result in foliation development. On the other hand, folding can continue until large values of shortening in a purely ductile regime, however, it is usually overprinted by pure shear deformation, foliation transposition, and/or boudinage. This may also have some implications for the evolution of fault propagation folds, where the folded layers are cut by underlying (thrust) faults after they have been shortened by about 30–40%. Before the critical shortening value, the limb dip and the area below the profile increase rapidly while the interlimb angle decreases accordingly; the changes of these parameters become increasingly slower after the critical value.

We speculate that folding close to constant arc length folding as part of the macroscopic shortening process can be active up to shortening values of about 30–40% under upper crustal conditions, before shortening by foliation development, faulting and other processes becomes dominant. Since the shortening taking place during folding can reach high values, it can constitute a major component of shortening in the upper continental crust such as for examples observable in the Zagros and other continental collision zones. In such areas, geometrical analyses of constant arc length folding allow estimating the bulk shortening taking place during folding.

References

Abbassi, M.R., Mancktelow, N.S., 1990. The effect of initial perturbation shape and symmetry on fold development. Journal of Structural Geology 12, 273–282.

Abbassi, M.R., Mancktelow, N.S., 1992. Single layer buckle in non-linear material – I. Experimental study of fold development from an isolated initial perturbation. Journal of Structural Geology 14, 85–104.

Aller, J., Bastida, F., Toimil, N.C., Bobillo-Ares, N.C., 2004. The use of conic sections for the geometrical analysis of folded surface profiles. Tectonophysics 379, 239–254.

Bastida, F., Aller, J., Bobillo-Ares, N.C., 1999. Geometrical analysis of folded surfaces using simple functions. Journal of Structural Geology 21, 729–742.

Bastida, F., Bobillo-Ares, N.C., Aller, J., Toimil, N.C., 2003. Analysis of folding by superposition of strain patterns. Journal of Structural Geology 25, 1121–1139.

Bastida, F., Aller, J., Bobillo-Ares, N.C., Toimil, N.C., 2005. Fold geometry: a basis for their kinematical analysis. Earth Science Reviews 70, 129–164.

Bastida, F., Aller, J., Toimil, N.C., Lisle, R.J., Bobillo-Ares, N.C., 2007. Some considerations on the kinematics of chevron folds. Journal of Structural Geology 29, 1185–1200.

Biot, M.A., 1961. Theory of folding of stratified viscoelastic media and its implications in tectonics and orogenesis. Geological Society of America Bulletin 72, 1595–1620.

Biot, M.A., 1964. Theory of internal buckling of a confined multilayered structure. Geological Society of America Bulletin 75, 563–568.

Biot, M.A., 1965a. Theory of similar folding of the first and second kind. Geological Society of America Bulletin 76, 251–258.

Biot, M.A., 1965b. Further development of the theory of internal buckling of multilayers. Geological Society of America Bulletin 76, 833–840.

Bobillo-Ares, N.C., Aller, J., Bastida, F., Lisle, R.J., Toimil, N.C., 2006. The problem of area change in tangential longitudinal strain folding. Journal of Structural Geology 28, 1835–1848.

Bobillo-Ares, N.C., Bastida, F., Aller, J., 2000. On tangential longitudinal strain folding. Tectonophysics 319, 53–68.

Carey, S.W., 1962. Folding. Journal of Alberta Society of Petroleum Geologists 10, 95–144.

Chamberlin, R.T., 1910. The Appalachian folds of central Pennsylvania. Journal of Geology 18-3, 228–251.

Chapple, W.M., 1964. A Mathematical Study of Finite Amplitude Rock-folding. Unpublished thesis, California Institute of Technology, 176 pp.

Chapple, W.M., 1968. A mathematical theory of finite-amplitude rock-folding. Geological Society of America Bulletin 79, 47–68.

Chapple, W.M., 1969. Fold shape and rheology: the folding of an isolated viscous-plastic layer. Tectonophysics 7, 97–116.

Connors, C., 1995. Determining heights and slopes of fault scarps and other surfaces on Venus using Magellan stereo radar. Journal of Geophysical Research 100 (14), 361–381.

Currie, J.B., Patnode, H.W., Trump, R.P., 1962. Development of folds in sedimentary strata. Geological Society of America Bulletin 73, 655–674.

Dahlstrom, C.D.A., 1990. Geometric constraints derived from the law of conservation of volume and applied to evolutionary models of detachment folding. American Association of Petroleum Geologists Bulletin 74, 336–344.

De Paor, D.G., 1996. Bézier curves and geological design in structural geology and personal computers. In: De Paor, D.G. (Ed.), Structural Geology and Personal Computers. Pergamon Press, Oxford, pp. 389–417.

de Sitter, L.U., 1956. Structural Geology. McGraw-Hill, London.

de Sitter, L.U., 1958. Boudins and parasitic folds in relation to cleavage and folding. Geologie en Mijnbouw 8, 277–286.

de Sitter, L.U., 1964. Structural Geology, second ed. McGraw-Hill, New York, 551 pp.

Dixon, J.M., Liu, S., 1992. Centrifuge modelling of the propagation of thrust faults. In: McClay, K.R. (Ed.), Thrust Tectonics. Chapman & Hall, London, pp. 53–69.

Ghent, R., Hansen, V., 1999. Structural and Kinematic analysis of Eastern Ovda Regio, Venus: implications for crustal plateau formation. Icarus 139, 116–136.

Goguel, J., 1962. Tectonics. Freeman, San Francisco, 348 pp.

Harbaugh, J.W., Preston, F.W., 1965. Fourier series analysis in geology. In: Symp. Comput. Appl. Miner. Explor. Tuscan, Ariz, V.I. Rl-R46.

Hudleston, P.J., 1973a. Fold morphology and some geometrical implications of theories of fold development. Tectonophysics 16, 1–46.

Hudleston, P.J., 1973b. An analysis of 'single layer' folds developed experimentally in viscous media. Tectonophysics 16, 189–214.

Hudleston, P.J., 1973c. The Analysis and interpretation of minor folds developed in the Moin rocks of Monar, Scotland. Tectonophysics 17, 89–132.

Hudleston, P.J., Treagus, S.H., Lan, L., 1996. Flexural flow folding: does it occur in nature? Geology 24, 203–206.

Jeng, F.S., Huang, K.P., 2008. Buckling folds of a single layer embedded in matrix – theoretical solutions and characteristics. Journal of Structural Geology 30, 633–648.

Jeng, F.S., Lai, Y.C., Teng, M.H., 2002. Influence of strain rate on buckle folding of an elasto-viscous single layer. Journal of Structural Geology 24, 501–516.

Johnson, A.M., Ellen, S.D., 1974. A theory of concentric, kink, and sinusoidal folding and of monoclinal flexuring of compressible, elastic multilayers. Part I, introduction. Tectonophysics 21, 301–339.

Johnson, A.M., Honea, E., 1975a. A theory of concentric, kink, and sinusoidal folding and of monoclinal flexuring of compressible, elastic multilayers. Part II, internal stress and nonlinear equations of equilibrium. Tectonophysics 25, 261–280.

Johnson, A.M., Honea, E., 1975b. A theory of concentric, kink, and sinusoidal folding and of monoclinal flexuring of compressible, elastic multilayers. Part III, transition from sinusoidal to concentric-like to chevron folds. Tectonophysics 27, 1–38.

Kobberger, G., Zulauf, G., 1995. Experimental folding and boudinage under pure constrictional conditions. Journal of Structural Geology 17, 1055–1063.

Kraus, J., Williams, P.F., 1998. Relationships between foliation development, porphyroblast growth and large-scale folding in a metaturbidite suite, Snow Lake, Canada. Journal of Structural Geology 20, 61–76.

Lisle, R.J., Fernandez Martınez, J.L., Bobillo-Ares, N., Menendez, O., Aller, J., Bastida, F., 2006. Fold profiler: a MATLAB—based program for fold shape classification. Computers & Geosciences 32, 102–108.
Mawer, C.K., Williams, P.F., 1991. Progressive folding and foliation development in a sheared, coticule-bearing phyllite. Journal of Structural Geology 13, 539–555.
Mertie, J.B., 1959. Classification, delineation and measurement of non-parallel folds. U. S. Geological Survey, Professional Paper 314-E, 91–124.
Mitra, S., 2003. A unified kinematic model for the evolution of detachment folds. Journal of Structural Geology 25 (10), 1659–1673.
Norris, D.K., 1963. Shearing strain in simple folds in layered media. Geological Survey of Canada, Paper 63 (2), 26–27.
Pollard, D.D., Fletcher, R.C., 2005. Fundamentals of Structural Geology. Cambridge University Press, Cambridge, 500 pp.
Ramsay, J.G., 1967. Folding and Fracturing of Rocks. McGraw-Hill Book Comp., New York, 568 pp.
Ramsay, J.G., 1974. Development of chevron folds. Geological Society of America Bulletin 85, 1741–1754.
Ramsay, J.G., Huber, M.I., 1997. Modern Structural Geology. In: Folds and Fractures, vol. 2. Academic Press, London, 700 pp.
Savage, H.M., Cook, L.C., 2003. Can flat-ramp-flat fault geometry be inferred from fold shape? A comparison of kinematic and mechanical folds. Journal of Structural Geology 25, 2023–2034.
Scharer, K.M., Burbank, D.W., Chen, J., Weldon, R.J., 2006. Kinematic models of fluvial terraces over active detachment folds: constraints on the growth mechanism of the Kashi-Atushi fold system, Chinese Tian Shan. GSA Bulletin 118 (7/8), 1006–1021.
Schmalholz, S.M., Podladchikov, Y.Y., 2000. Finite amplitude folding: transition from exponential to layer length controlled growth. Earth and Planetary Science Letters 181 (4), 619–633.
Schmalholz, S.M., Podladchikov, Y.Y., Burg, J.-P., 2002. Control of folding by gravity and matrix thickness: implications for large-scale folding. Journal of Geophysical Research 107 (B1), 2005. doi:10.1029/2001JB000355.
Schmalholz, S.M., Schmid, D.W., Fletcher, R.C., 2008. Evolution of pinch-and-swell structures in a power-law layer. Journal of Structural Geology 30, 649–663.
Schmalholz, S.M., 2006. Scaled amplification equation: a key to the folding history of buckled viscous single-layers. Tectonophysics 419, 41–53.
Sengupta, S., 1983. Folding of boudinaged layers. Journal of Structural Geology 5, 197–210.
Sherwin, J., Chapple, W.M., 1968. Wavelengths of single layer folds: a comparison between theory and observation. American Journal of Science 266, 167–179.
Stabler, C.L., 1968. Simplified Fourier analysis of fold shapes. Tectonophysics 6, 343–350.
Twiss, R.J., 1988. Description and classification of folds in single surfaces. Journal of Structural Geology 10, 607–623.
Vacas Peña, J.M., Martínez Catalan, J.R., 2004. A computer program for the simulation of folds of different sizes under the influence of gravity. Computers & Geosciences 30, 33–43.